The inhomogeneous reionization of the local intergalactic medium by metal-poor globular clusters

Article (Published Version)

Monthly Notices
of the
ROYAL ASTRONOMICAL SOCIETY

MNRAS **431,** 3087–3102 (2013) doi:10.1093/mnras/stt382
Advance Access publication 2013 April 3

The inhomogeneous reionization of the local intergalactic medium by metal-poor globular clusters

B. F. Griffen,[1]⋆ M. J. Drinkwater,[1] Ilian T. Iliev,[2] P. A. Thomas[2] and Garrelt Mellema[3]

[1]*Department of Physics, University of Queensland, QLD 4072, Australia*
[2]*Astronomy Centre, University of Sussex, Falmer, Brighton BN1 9QH, UK*
[3]*Department of Astronomy and Oskar Klein Centre, AlbaNova, Stockholm University, SE-10691 Stockholm, Sweden*

Accepted 2013 February 27. Received 2013 February 26; in original form 2012 September 25

ABSTRACT

We present detailed radiative transfer simulations of the reionization of the Milky Way by metal-poor globular clusters. We identify potential metal-poor globular cluster candidates within the Aquarius simulation using dark matter halo velocity dispersions. We calculate the local ionization fields via a photon-conserving, three dimensional non-equilibrium chemistry code. The key feature of the model is that globular cluster formation is suppressed if the local gas is ionized. We assume that at these early times, the ionization field is dominated by the flux from metal-poor globular clusters.

Our spatial treatment of the ionization field leads to drastically different numbers and spatial distributions when compared to models where globular cluster formation is simply truncated at early redshifts ($z \sim 13$). The spatial distributions are more extended and more globular clusters are produced. We find that additional sources of ionization are required at later epochs ($z \sim 10$) to ionize the remaining gas and recover radial distributions statistically consistent with that of the Milky Way metal-poor globular clusters.

We investigate a range of plausible ionization efficiencies to determine the effect photon-rich and photon-poor models have on present-day globular cluster properties. If globular clusters do indeed form within high-redshift dark matter haloes, they produce enough photons to ionize 98 and 90 per cent local (i.e. $2^3\ h^{-3}$ Mpc^3 centred on the host galaxy) volume and mass by redshift 10, respectively. In our photon-poorest model, this contribution drops to 60 and 50 per cent. Our model therefore implies that globular clusters are important contributors to the reionization process on local scales at high-redshift until more photon-rich sources dominate the photon budget at later times. The surviving clusters in all models have a narrow average age range (mean = 13.34 Gyr, $\sigma = 0.04$ Gyr) consistent with current age estimates of the Milky Way metal-poor globular clusters. We also test a simple dynamical destruction model and estimate that ∼60 per cent of all metal-poor globular clusters formed at high redshift have since been destroyed via tidal interactions with the host galaxy.

Key words: galaxy: formation – globular clusters: general – intergalactic medium – cosmology: theory.

1 INTRODUCTION

It is now well understood that the Universe emerged from the so-called *dark ages* ($30 < z < 1100$; Rees 1997) when light from the first stars and quasars ignited and radiated large quantities of ionizing photons into the intergalactic medium (IGM). This radiation reionized the universe in two epochs: one for hydrogen ($7 < z < 15$; see Loeb & Barkana 2001 for a review), and one for helium ($z \sim 3.5$; Davidsen, Kriss & Zheng 1996). Though the most likely sources of helium reionization are quasars, the sources of hydrogen reionization are far less well known. Possible sources of high-redshift reionization include Population III stars (Bromm & Larson 2004 and Wise 2012 and references therein), Population II stars (e.g. Sokasian et al. 2003), quasars (Madau, Haardt & Rees 1999; Fan et al. 2001, 2006) and more recently, particle decay/annihilation (Mapelli, Ferrara & Pierpaoli 2006). Recent work (Conroy, Loeb & Spergel 2011; Schaerer & Charbonnel 2011) suggests that initial stellar masses of today's ancient globular clusters (hereafter GCs) could have been as much as 8–25 times higher when they first formed, reinforcing earlier conclusions that metal-poor GCs (hereafter MPGCs) could have significantly contributed to the reionization of the IGM at high redshift. Ricotti & Shull (2000) were among the first to formally suggest that GCs could have supplied a large quantity of the

⋆ E-mail: brendan.f.griffen@gmail.com

ionizing radiation. Several simulation studies have estimated the GC contribution (Ricotti 2002; Ricotti & Ostriker 2004; Power et al. 2009).[1] These studies were limited by uncertain parameters (e.g. star formation efficiencies, escape fractions, photoionization rates) and lacked the resolution to resolve GC formation sites, but they all concluded that the flux from the first generation of GCs could have significantly contributed to the reionization of the Milky Way.

The common approach used in many studies of GC formation (e.g. Bekki 2005; Moore et al. 2006) is to *force* a truncation redshift (after which no more GCs form), giving satellite numbers and distributions comparable to observations. Whilst this approach can reproduce some observables, it does not account for the spatial inhomogeneity of the ionization field whereby sources are suppressed at different places and at different times. Ciardi, Stoehr & White (2003), Furlanetto, Zaldarriaga & Hernquist (2004), Barkana (2004) and Iliev et al. (2006) all clearly demonstrated that the reionization process was in fact extended in time and spatially inhomogeneous resulting in vastly different reionization times for different areas of the Universe. If studies of GC formation neglect the inhomogeneity of reionization field, their models will result in inaccurate formation numbers and distributions.

Over the years, many have studied the connection between the reionization epoch and satellite formation. Alvarez et al. (2009) combined an *N*-body simulation with three-dimensional reionization calculations (1 h^{-1} Gpc width) to determine the relationship between reionization history and local environment. They found that on average, haloes with mass less than 10^{13} $M_{\odot}$ were reionized internally, whilst almost all haloes with mass greater than 10^{14} $M_{\odot}$ were reionized from without (consistent with Ocvirk & Aubert 2011). Busha et al. (2010) combined the subhalo catalogues from the Via Lactea II simulation with a Gpc-scale *N*-body simulation and found that by varying the reionization time over the range expected for Milky Way mass haloes it could change the number of satellite galaxies by roughly two to three orders of magnitude.

The work of Alvarez et al. (2009) and Busha et al. (2010) were semi-analytic studies of the reionization epoch. Iliev et al. (2011), however, combined a cosmological simulation with radiative transfer (RT) in a model of the Local Group and nearby clusters. They found that for photon-poor models, the Local Group could have been reionized by itself (photon-rich models found that nearby clusters reionized the Local Group externally). Lunnan et al. (2012) combined three-dimensional maps of reionization (using the semi-analytic models of Furlanetto et al. 2004) with the initial density field of the *Aquarius* simulation (Springel et al. 2008). They found that the number of satellites depends sensitively on the reionization model, with a factor of 3–4 difference for a given host halo. Most recently and perhaps most intriguingly, Boylan-Kolchin, Bullock & Kaplinghat (2011) have found that dissipationless dark matter simulations predict that the majority of the most massive subhaloes of the Milky Way are too dense to host any bright satellites at all. The vast majority of these works primarily focus on the effect of patchy reionization on the satellite (dwarf) systems of the Milky Way. All of them, however, exclude the contributions from primordial GCs. Whilst all of these studies show the consequences of a patchy reionization process on galaxy evolution, a model incorporating both this process and *all* of the relevant reionization sources is yet to be carried out.

[1] Although Power et al. (2009) only considered the contribution of X-ray binaries within GCs.

Griffen et al. (2010, hereafter G10) recently used cosmological simulations (Aquarius) to study the reionization of the Milky Way by MPGCs. They concluded that with a reasonable escape fraction and star formation rate, the primordial MPGCs of the Milky Way could have ionized the Milky Way by as early as $z \sim 13$. They found that the UV flux from high-z GCs had drastic consequences for not only the spatial and dynamical properties of present-day ($z = 0$) GCs, but also for their overall ages as well. The main caveats of their work, however, were (i) they assumed that *all* photons emitted from a potential MPGC would contribute to the reionization of the Milky Way (much of the UV flux would have escaped into the outer IGM), (ii) they did not model the dynamical destruction of the GCs once they merged with the central halo and (iii) did not allow for delayed star formation to take place whereby a previously suppressed halo could reignite if the recombinations were high enough and/or it became neutral later.

In this paper, we extend the methods employed by G10, addressing all the major caveats. We do this by (i) modelling a spatially dependent reionization process by calculating the propagation of ionization fronts *directly* with a ray-tracing RT code (C^2-RAY; Mellema et al. 2006), (ii) measuring the effects of dynamical destruction on present-day ($z = 0$) GC properties by combining the Aquarius data with dynamical models (Baumgardt & Makino 2003) and (iii) allowing for delayed star formation by combining the spatial information of haloes within the Aquarius merger trees with the state of the IGM as modelled by C^2-RAY. We aim to quantitatively analyse the formation of primordial GCs in a Milky Way-type environment and determine to what extent GCs contributed to the reionization of the IGM and how the their contributions affected present day properties of MPGCs. We focus on testing the dark matter halo formation hypothesis for metal-poor GCs. As in G10, we assume that the ionizing flux from MPGCs dominates the IGM at early times. This means the only sources of reionization in our study are those MPGC candidates identified via our selection criteria.

This paper is organized as follows: Section 2 describes how we identify GC candidates in the Aquarius dark matter simulation and the RT code used to model MPGCs as sources of reionizing radiation. Section 3 describes the extensions to our model which include dynamical destruction and delayed star formation. Section 4 describes our results, exploring several scenarios to better understand the consequences of high and low escape fractions, halo concentrations, dynamical destruction and delayed star formation on present day ($z = 0$) properties of our GC candidate clusters. Section 5 discusses the consequences of this work in the wider context of galaxy evolution and large-scale reionization. Section 6 describes the primary conclusions of this paper including a discussion of the caveats of this work and avenues for future study.

2 METHODOLOGY

In this section, we describe the details of our methodology. We begin by summarizing the relevant details of our data set: the Aquarius simulation. We then describe how we identify GC candidates using the Aquarius merger trees and lastly, we describe how we model GCs as ionizing sources.

2.1 The Aquarius simulations

The Aquarius suite consists of six different simulations of Milky Way-sized galaxies, one of which is used here. A more detailed description of the simulation can be found in Springel et al. (2008), but we review the details relevant to this work here.

Table 1. The basic parameters of the Aquarius simulation data used in this paper.

Name	m_p ($M_\odot$)	ϵ (pc)	N_{hr}	N_{lr}	M_{200} ($M_\odot$)	r_{200} (kpc)	M_{50} ($M_\odot$)	r_{50} (kpc)	N_{50}
Aq-A2	1.370×10^4	65.8	531 570 000	75 296 170	1.842×10^{12}	245.88	2.524×10^{12}	433.52	184 243 536

Notes. m_p is the particle mass, ϵ is the Plummer equivalent gravitational softening length, N_{hr} is the number of high-resolution particles and N_{lr} the number of low-resolution particles filling the rest of the volume. M_{200} is the virial mass of the halo, defined as the mass enclosed in a sphere with mean density 200 times the critical value. r_{200} gives the corresponding virial radius. We also give the mass and radius for a sphere of overdensity 50 times the critical density, denoted as M_{50} and r_{50}. Note that this radius encloses a mean density 200 times the background density. Finally, N_{50} gives the number of simulation particles within r_{50}.

The Aquarius suite has same cosmological initial conditions as that of the Millennium simulation (Springel et al. 2005). The initial size of the periodic box was 100 h^{-1} Mpc set in a cosmology of $\Omega_m = 0.25$, $\Omega_\Lambda = 0.75$, $\sigma_8 = 0.9$, $n_s = 1$ and Hubble constant $H_0 = 100\ h$ km s^{-1} Mpc^{-1} = 73 km s^{-1} Mpc^{-1}. We are aware that the value of $\sigma_8 = 0.9$ is higher than the currently accepted valued of σ_8 and could lead to an overestimate of the ages of all candidates since *all* haloes will form at earlier times. In terms of reionization, this means that for a fixed ionizing emissivity proportional to the collapsed fraction, the evolution is shifted to somewhat earlier times, resulting in an earlier overlap epoch (Alvarez et al. 2006). Studies by Boylan-Kolchin et al. (2011) predict that this would have a relatively minor effect.

The Millennium simulation was searched for haloes of roughly Milky Way mass and without massive close neighbours in the present day ($z = 0$). Springel et al. (2008) also checked that the semi-analytic modelling applied to the target haloes predicated them to host late-type galaxies. Otherwise the selection was random. These were then resimulated using 900^3 particles in a box of dimension 100 h^{-1} Mpc. After identifying the Lagrangian region from when each halo formed, the mass distribution was rerun at a much higher spatial and mass resolution. Although coarse particles were used to sample the distant regions, the resolution was such that the tidal field was accurately resolved at all times.

The haloes labelled 'Aq-A' to 'Aq-F' stored snapshots at 128 output times equally spaced in log (a), where $a = 1/(1 + z)$ represents the expansion factor (between redshift between $z = 127$ and $z = 0$). In this paper, we only focus on the highest resolution halo available, AqA2. Dark matter haloes were identified using a combination of the friends-of-friends algorithm and SUBFIND (Springel et al. 2001). As described in Cole et al. (2008), haloes and their substructure are traced through the snapshots and linked together in a merger tree. The smallest halo able to be resolved in the simulation is of the order the 10^5 $M_\odot$. The most relevant details of the Aquarius simulation for this study are shown in Table 1.

2.2 Identifying primordial GCs

The precise mechanism by which primordial GCs form is still largely unknown. Peebles (1984) was one of the first to suggest that GCs may have formed within extended dark matter haloes at high redshift. Observations of thin tidal tails by Grillmair et al. (1995) and Odenkirchen et al. (2003) drastically reduced the popularity of this model (Moore 1996 found that tidal tails should not exist if GCs are in extended haloes). These studies, however, assume that GCs at the *present* period represent the environment from which they were born. There is currently no solid evidence to suggest that because GCs today are not observed to contain significant traces of dark matter, their more massive progenitors did not form within dark matter haloes.

More recent work has renewed interest in the dark halo–GC formation scenario due to numerical models published over the past decade. From a dynamical evolution standpoint, if GCs were 8–25 times larger when formed than observed at present (Schaerer & Charbonnel 2011), the likelihood of a giant molecular cloud ($f_{sfe} \sim 0.3$) of $\sim 10^9$ $M_\odot$ collapsing *without* being embedded within any dark halo is at this stage, small. Bromm & Clarke (2002) and Mashchenko & Sills (2005) have also shown that it is possible for the extended haloes of GCs to be tidally stripped away by the present day. More recently, Boley et al. (2009) carried out studies of the radial distribution of bright GCs in the Milky Way and concluded that it is possible that they formed in biased dark matter haloes at high redshift. The formation of multiple stellar populations within GCs (Bekki & Yahagi 2006; Bekki et al. 2007; Carretta et al. 2010) are also consistent with the dark halo–GC formation channel.

In our work, we assume that high-z GCs *did* form within the very first collapsed minihaloes and due to dynamical disruption and violent relaxation have since lost their dark matter haloes. This assumption also makes it possible to model them as sources of reionization in current dark matter only, Λ cold dark matter simulations relatively straightforwardly.

Our primary model of GC formation is the same as that found in Section 2.2 of G10. In this work, however, we focus on MPGC production only but significantly improve on the previous work. We focus on MPGC formation because their relative spread of ages (De Angeli et al. 2005) places them coincidentally at the ideal time to be significant contributors to the reionization process.

We adopt a relatively simple model to identify where the MPGC objects would form within the Aquarius simulation based on the requirements for the collapse of a proto-GC gas cloud. The majority of previous studies adopt a similar model for GC formation, but the resolution of the Aquarius simulation allows us to *directly* measure the primary parameter: temperature.

Nishi (2002) and several others found that in order for gas clouds to efficiently cool, they must facilitate one or a combination of the three mechanisms: collisional excitation of hydrogen and helium, radiative recombination of hydrogen and bremsstrahlung. The typical cooling function for a proto-GC candidate reveals an immense increase in the cooling rate as the temperature reaches 10^4 K, critical to the formation of stars.

Assuming that the gas is in quasi-static equilibrium with the dark matter, we can use the virial theorem to relate the 1D velocity dispersion of the dark matter haloes to temperature. The ratio of the 1D internal velocity dispersion of the dark matter subhaloes (σ_v) to the *inferred* virial temperature of the gas, T_v is given by

$$\sigma_v^2 = \frac{kT_v}{\mu m_H}, \quad (1)$$

where m_H is the mass of a hydrogen atom and μ is the mean molecular weight of the gas. We adopt molecular weight of $\mu = 0.58$,

appropriate for a fully ionized, primordial gas. Using these values, we therefore assume that whenever a halo's velocity dispersion increased *above* 11.9 km s^{-1} ($T_v \sim 10^4$ K), it is a *GC candidate*. The smallest halo identified via this method contains 1619 particles, corresponding to a dark matter mass of 2.17×10^7 M$_\odot$. Throughout this work, 'MPGCs' and 'GCs' represent the exact same objects, metal-poor GCs. Whilst some of these objects will invariably evolve into dwarf satellites, the objects we focus on in this work are only those which merge with the central halo by the present day. In all of the following comparisons with observations, we use the 2010 edition of the GC catalogue created by Harris (1996).

2.3 Treatment of GCs as ionizing sources

The Aquarius simulation allows us to identify where and when candidate sources (i.e. GCs) will form and our photon-conserving, three-dimensional, non-equilibrium chemistry code (C^2-RAY; Mellema et al. 2006) will ensure that the radiation from these sources is treated accurately.

2.3.1 RT Calculations

C^2-RAY is a grid-based short characteristics ray-tracing code which is photon conserving and traces rays away from our GC sources up to each cell. Photon conservation is assured by adopting a finite-volume approach when calculating the photoionization rates and by using time-averaged optical depths. Although helium is not modelled directly in this work, C^2-RAY assumes that where and when hydrogen is ionized, helium is once (but not twice) ionized because of the similar ionization potentials of hydrogen and helium-I. The evolution of the ionized fraction of hydrogen, $x_{\rm i}$, (including recombinations) is governed by

$$\frac{{\rm d}x_{\rm i}}{{\rm d}t} = (1 - x_{\rm i})(\Gamma_{\rm i} + n_{\rm e} C_{\rm i}) - x_{\rm i} n_{\rm e} \alpha_{\rm B}, \quad (2)$$

where $n_{\rm e}$ is the electron density, $\Gamma_{\rm i}$ is the photo-ionization rate, $C_{\rm i}$ is the collisional ionization rate and $\alpha_{\rm B}$ is the recombination rate. The code has been tested against nine other rival ray-tracing codes and was found to be on par with the best codes available today (Iliev et al. 2006, 2009). For more details, see Mellema et al. (2006) and references therein.

A density mesh at both 256^3 and 512^3 resolutions of the AqA2 halo was created for each time-step using a Cloud-in-Cell algorithm centred on the central host maintaining a physical volume of $6\,h^{-1}$ Mpc. This means that the cell width for our high-resolution run is 11 h^{-1} kpc/cell, significantly more accurate than the 195 h^{-1} kpc per cell used in Lunnan et al. (2012). Since the Aquarius simulation consists of both high- and low-resolution particles in the same volume, composite positions of all types of particles were used to ensure the density was properly represented at all spatial scales.

2.3.2 Mapping sources

Potential GC formation sites were located via the prescription previously discussed (see Section 2.2) through SQL queries of the publicly availably Aquarius data base.[2] These were then mapped into a grid-based mesh for radiative processing according to the run's resolution. If more than one halo was identified within the same cell, those haloes were combined and a luminosity assigned following a prescription based on their combined mass. For the 256^3 simulation, we found that only eight GC candidates formed within the same cell as another. When the resolution was increased to 512^3, no two GCs were found to have formed within the same grid cell.

The completeness of the identified sources is not homogeneous across the C^2-RAY box. Since the Aquarius volume was resimulated in a Lagrangian volume, the total volume in which sources can be identified is *less* than the total volume of the box used by C^2-RAY. This incompleteness near the edges is yet another reason to restrict analysis to only those sources which have merged with the central halo. Despite having minor source incompleteness just near the edge of the C^2-RAY volume, the density field in these outer regions is still accurately represented since the particles which created the mesh span the entire volume (high resolution and low resolution).

2.3.3 Calculating the total ionization efficiency, f_γ

As highlighted by Ricotti (2002) and Schaerer & Charbonnel (2011), the primary problem with all GCs studies is that there is significant uncertainty in the emissivity of GCs in the early universe. Exactly how many photons are produced in GCs over time depends largely on three parameters: what fraction of the gas is converted into stars $f_{\rm sfe}$, how effective are the stars at producing ionizing photons $\bar{q}$, which reach the IGM and finally, what fraction of the photons manage to escape the collapsing giant molecular cloud $f_{\rm esc}$. We parametrize all of these with a single parameter, f_γ ($f_\gamma = \bar{q} \times f_{\rm sfe} \times f_{\rm esc}$) which is equivalent to the number of ionizing photons per atom entering the IGM (between time-steps). Since the code is sufficiently fast and the number of ionizing sources is relatively small, several runs of varying f_γ values were able to be completed.

Baumgardt & Kroupa (2007) found that in order to form a bound cluster, the star formation efficiency (SFE) had to be one third or more. If all of the gas in a halo does not end up in the proto-cluster, the SFE could be considerably lower. The range of plausible values of the SFE adopted were $0.15 < f_{\rm sfe} < 0.7$.

Yajima, Choi & Nagamine (2011) recently combined three-dimensional RT calculations and a cosmological smooth particle hydrodynamic simulation to study the escape fraction, $f_{\rm esc}$, of ionizing photons of high-redshift galaxies. Though they did not specifically study MPGCs, they found that the escape fraction drastically increased towards decreasing mass with haloes of mass $<10^9$ M$_\odot$ having an average $f_{\rm esc} \sim 0.4$. Ferrara & Loeb (2012) have recently studied the ionization escape fraction of low-mass haloes and found that very high escape fractions ($f_{\rm esc} \sim 1$) are only possible for low-mass haloes ($M < 10^{8.7}$M$_\odot$) which is consistent with previous studies (Wise & Cen 2009). We combine this with the previous work (Ricotti & Shull 2000; Ricotti 2002; Ricotti & Ostriker 2004) to adopt a reasonable escape fraction range of $0.1 < f_{\rm esc} < 0.7$. We do not adopt the extreme upper limit of $f_{\rm esc} = 1$, since dust extinction and large levels of radiation absorbed by molecular clouds make this unlikely (Ricotti 2002).

As in G10, we use the Population II efficiency curve of fig. 2 from Tumlinson, Venkatesan & Shull (2004) (calculated using the STARBURST99 code of Leitherer et al. 1999) to calculate the number of ionizing photons emitted per baryon. Averaging over a Salpeter IMF (see appendix of G10) gives $\bar{q} \approx 10\,000$. This figure could be raised by moving towards a more top-heavy initial mass function (IMF) but recent work by Schaerer & Charbonnel (2011) indicates

[2] Aquarius data base: http://www.galaxy-catalogue.dur.ac.uk :8080/Aquarius/

Table 2. The photon-poorest and photon-richest scenarios constrained by previous computational studies. These limits set the upper and lower bounds on the total number of photons per baryon leaving a proto-GC, f_γ, in this study.

Parameter	Photon-poorest model	Photon-richest model
$\bar{q}$	10 000 ph/b	10 000 ph/b
$f_{\rm sfe}$	0.15	0.7
$f_{\rm esc}$	0.1	0.7
f_γ	150 ph/b	∼5000 ph/b

that the ionizing photon output is quite independent of the IMF slope.

Since there are relatively few observational constraints on the escape fraction and SFE at high redshift, the total ionization efficiency, f_γ, is largely a free parameter with significant uncertainty. However, by spanning a wide range of photon efficiencies, the state of the IGM during reionization can be examined without having *exact* knowledge of which efficiency model (photon rich or photon poor) should be adopted. The upper and lower limits of the total number of photons per baryons being produced by GC candidates in this study can be found in Table 2. The total range of f_γ values used in this study, ranging from extremely photon poor to extremely photon rich, are $f_\gamma = 150, 250, 500, 700, 1000$ and 5000 photons per baryon. Our primary assumption here is that the baryons follow the underlying dark matter and photons are produced uniformly over a given time-step. Any unsuppressed sources will continue producing photons in the subsequent time-step. Each simulation has a time-step of ∼20 Myr.

In addition to the ionization models already described, we include a 'truncation model' whereby halo formation is suppressed beyond a fixed redshift ($z_{\rm trunc}$). The only other requirement for these haloes is that they have merged with the central halo by the present day ($z = 0$). G10 originally used this type of suppression model and found a $z_{\rm trunc} = 13$ to be the most suitable of the possible truncation redshifts. This truncation redshift can ultimately be arbitrary as it simply depends on the efficiency of the sources used. We adopt $z_{\rm trunc} = 13$ here for the simple purpose of illustrating the effect inhomogeneous ionization models have on the numbers and distributions of GC candidates when compared to a truncation models.

2.3.4 Suppression criterion

We define 'suppression' as the inability of candidate haloes to develop into GCs because their gas content is ionized *locally*. An RT cell is considered ionized when the ionized fraction of hydrogen is above a fixed threshold ($x_{\rm thresh}$). Throughout our entire study, we set $x_{\rm thresh} = 0.1$. GC candidates residing in a cell with an ionized fraction above this threshold are suppressed.

Iliev et al. (2012) (in Appendix B) examined the effect of varying the suppression threshold. They found that both $x_{\rm thresh} = 0.1$ and 0.5 yield the same IGM evolution, apart from a slight offset in time. Only for $x_{\rm thresh} = 0.9$ (weak suppression) does the evolution of the IGM begin to behave very differently. However, they were studying reionization in large-scale galaxy cluster environments and so the conclusion does not necessarily apply to the smaller Milky Way-type environment studied here. The only way to determine the effect of higher ionized thresholds is to recalculate one of the runs presented here with higher thresholds. We defer this to future work (see Section 5). In *this* work, our condition for GC formation is that a halo is for the first time above $\sigma > 11.9$ km s^{-1} and that it resides within a cell with an ionized fraction, $x < 0.1$.

We also add another criterion which is based on mass. We assume that candidate GCs with formation masses above 10^9 M$_\odot$ are not suppressed by radiation and are thus active sources at all times, regardless of the state of the gas around them (Iliev et al. 2007). This selection criteria only affects five candidate haloes in our study as the vast majority of them form with masses $<10^9$ M$_\odot$.

3 MODEL EXTENSIONS: DELAYED STAR FORMATION AND DYNAMICAL DESTRUCTION

In this section, we detail two extensions of the previous model: delayed star formation and dynamical disruption. Whilst these processes have been studied before, it is the first time that the following two models have been combined together in the context of GC formation.

3.1 Delayed star formation

In many previous works, the suppression of candidate clusters is achieved with a simple prescription: if a candidate satellite resides in an ionized region, it is suppressed permanently. We adopt this technique for some of our models and class them as 'Model 1' or the 'permanently suppressed' model.

On cosmological scales, such 'suppressed once-and-forever' models are a good approximation since there are many neighbouring sources to keep each region ionized. Any descendent of a suppressed halo entering one of these ionized regions will remain suppressed. On small scales, however, such as the one being dealt with here, there are occasions where a candidate GC, previously suppressed, may be able to become active again once its gas content becomes neutral at a later time-step. This process effectively delays the star formation of a GC candidate and adds previously suppressed candidates to the list of legitimate GCs in the present day ($z = 0$). This important process can be closely examined by using the merger trees of the simulation under study. In this work, we denote this type of model as 'Model 2' or the 'delayed' model. These names are used interchangeably though out this work.

Our delayed model works as follows. At each snapshot, we add the descendent IDs of each of the active haloes to a cumulative list. In the subsequent snapshot, candidate haloes are checked against this list to determine if any of the potentially active sources have been active before. If a match is found, this halo's descendent ID is added to the list and it is removed from the potential new sources for that snapshot. If a match is not found, the ionization state of the cell that source resides in is checked and if it is neutral (or below $x_{\rm thresh} = 0.10$), it will then become active and the usual quantities propagated.

In this way, Model 2 has two types of populations forming over the course of the simulation: 'first timers' (i.e. source which becomes active in the same snapshot they are identified) and 'delayed' (i.e. they become active at a later snapshot than the one they are identified). This also self-consistently excludes any haloes which have *any* active ancestors. At early times, one would expect there to be direct overlap of the total number of sources using either Model 1 and Model 2 but once delayed haloes add substantial ionizing photons to the IGM at later times, this will alter the number and present-day properties of the candidates across the two models.

Table 3. The simulation suites used in this study. 'M1' and 'M2' denote Model 1 (permanently suppressed model) and Model 2 (delayed model), respectively. Our fiducial model is M1_512_ph500. A lower resolution run (256^3) of our fiducial model is also carried out to test for convergence to ensure that our results are not resolution dependent (see Section 5.3).

Name	Number of cells	f_γ (ph/b)
M1_512_ph150	512^3	150
M1_512_ph250	512^3	250
M1_256_ph500	256^3	500
M1_512_ph500	$\mathbf{512^3}$	**500**
M1_512_ph700	512^3	700
M1_512_ph1000	512^3	1000
M1_512_ph5000	512^3	5000
M2_512_ph150	512^3	150
M2_512_ph250	512^3	250
M2_512_ph500	512^3	500
M2_512_ph700	512^3	700
M2_512_ph1000	512^3	1000
M2_512_ph5000	512^3	5000

In summary, Model 1 represents a 'permanently suppressed' scenario whereby ionization suppresses a GC candidate permanently and *never* ignites at any subsequent time-step. Model 2 (or 'delayed model') incorporates all of the same identification methods used in Model 1 except that now the descendents of previously suppressed haloes can become active if their gas content becomes sufficiently neutral and they have no active ancestors.

We adopt Model 1 with $f_\gamma = 500$ (where $f_{\rm esc} = 0.2$ and $f_{\rm sfe} = 0.25$) as our fiducial model because the adopted total escape fraction is within the reasonable range of literature estimates. Table 3 lists the two types of models tested and the range of photoionization efficiencies adopted in this work (e.g. our fiducial model is represented by M1_512_ph500: Model 1 at 512^3 resolution with $f_\gamma = 500$).

3.2 Dynamical destruction

The second extension to our model addresses dynamical destruction. Although we have excellent resolving power to locate where candidates form, it is impossible to locate these halo structures in the present day ($z = 0$) as the vast majority of them will have undergone mergers with either the host or each other. As with G10, we assume that the collapsed baryonic gas fraction of a GC at the centre of each halo will follow the same trajectory as that of the most bound particle of the halo. At each snapshot, we simply identify the most bound particle corresponding to each GC candidate. We then follow this most bound particle through to the present day allowing us to track the GC formation sites over the course of the entire simulation.

During mergers with the central halo, the formation site is no longer tracked by SUBFIND so we infer the trajectory of the formation site within the host halo based on the most bound particle alone. Baumgardt & Makino (2003) derived a fitting formula based on a series of *N*-body models to determine whether a star cluster, given a few basic orbital characteristics, will be disrupted during its orbit around a host after such an encounter takes place. Their equation 10 gives the dissolution time as

$$T_{\rm diss} = \beta \left[\frac{M}{0.33\ {\rm M}_\odot}\right]^x \frac{R_{\rm G}}{\rm kpc} \left(\frac{V_{\rm G}}{220\ {\rm km\ s^{-1}}}\right)^{-1} (1-\epsilon), \qquad (3)$$

where M is the halo mass before infall, ϵ is the orbital eccentricity, $R_{\rm G}$ is the apocentric distance of the halo (kpc), $V_{\rm G}$ is the circular velocity (km s^{-1}) of the host galaxy and x and β are cluster scaling law parameters depending on the cluster concentration. From a fit to the lifetimes of the King (1966) models with dimensionless central potential W_0=5.0, Baumgardt & Makino (2003) found $x = 0.75$, $\beta = 1.91$.

We traced the position of the most bound particle of each candidate clusters during its merger with the host halo to measure the eccentricity of the orbit ϵ and the apocentric distance $R_{\rm G}$.

For more concentrated $W_0 = 7.0$ King profile clusters, they found a small change in the dissolution time of a cluster (see fig. 3 of Baumgardt & Makino 2003 for details) and so for the sake of simplicity we restrict our dissolution analysis to $W_0 = 5.0$ King profile clusters only. In order to determine whether a candidate GC survives an encounter with the central host halo, its calculated dissolution time must be compared to the time it merged with the central host. If the time since the candidate GC merged with the central halo exceeds its dissolution time, then the cluster is disrupted.

4 RESULTS

Here, we present the results for Model 1 (Section 4.1): dynamical destruction applied to Model 1 (Section 4.2) and Model 2 (Section 4.3).

The objects used in all of the following analyses have been restricted to only those which merge with the final host by $z = 0$. Specifically, *merged* means that SUBFIND can no longer recognize them as two separate structures in the present day. The total number of objects formed without suppression is 310. Though there are objects which retain their dark matter haloes, we cite G10 as a preliminary analysis of these objects and save more detailed study of these survivors for future work.

4.1 Model 1: 'suppressed permanently'

4.1.1 Visualization of the ionization field

We identify GCs using the method described in Section 2.2 and show a visual representation of these candidates ionizing the IGM in Figs 1 and 2. Fig. 1 shows the neutral gas density using a fixed emissivity of $f_\gamma = 500$ photons per baryon at $z = 14.03, 12.07, 8.90, 7.03$ within a box of $6^3\ h^{-3}$ Mpc^3. This shows a clear evolution of the ionizing fronts throughout the IGM during the formation of the proto-Milky Way particularly highlighting the inhomogeneous nature of the ionization field. Fig. 2 shows six runs at differing emissivities all captured at the same time ($z = 10.11$). The emissivities range from $f_\gamma = 150$ to $f_\gamma = 5000$ and clearly illustrates how higher photoionization efficiencies ionize larger volumes. Interestingly, the very central regions of the host galaxy remain relatively neutral ($R < 100$ kpc). An increase in the local recombination rate ($\propto \rho^2$) in this region makes it difficult for central region to become ionized.

4.1.2 Formation history and numbers

The formation history and overall numbers in each of our models are shown in Fig. 3. GC formation *without* suppression is shown by the open bins outlining each of the suppression models (shown in colour). As expected, the relative numbers of objects at high redshift are similar as the formation environments are roughly the same. As the activation of more sources proceeds, large quantities

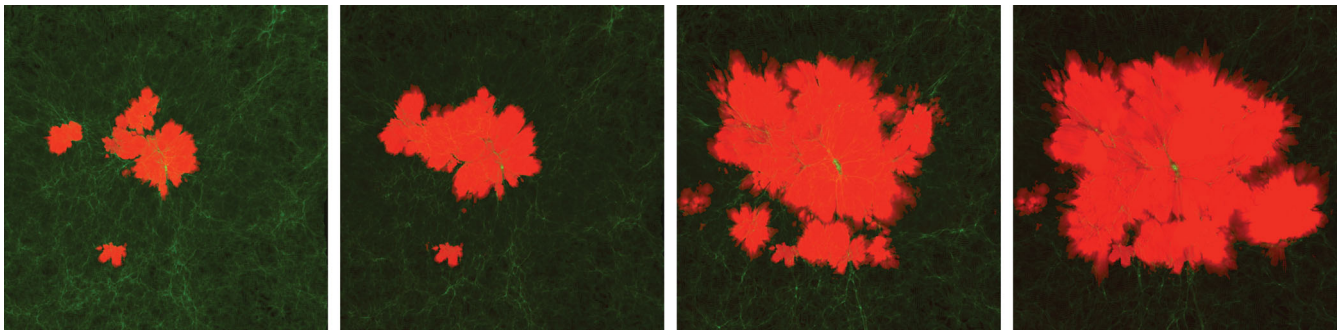

Figure 1. Time evolution of the ionization field. Each panel represents a spatial slice (x–y projection), 460 h^{-1}kpc thick, of the ionized and neutral gas density from simulations of Model 1 using photoionization efficiencies of $f_\gamma = 500$ at $z = 14.03$, 12.07, 8.90 and 7.03, respectively. The box in each panel has a comoving width of 6 h^{-1} Mpc.

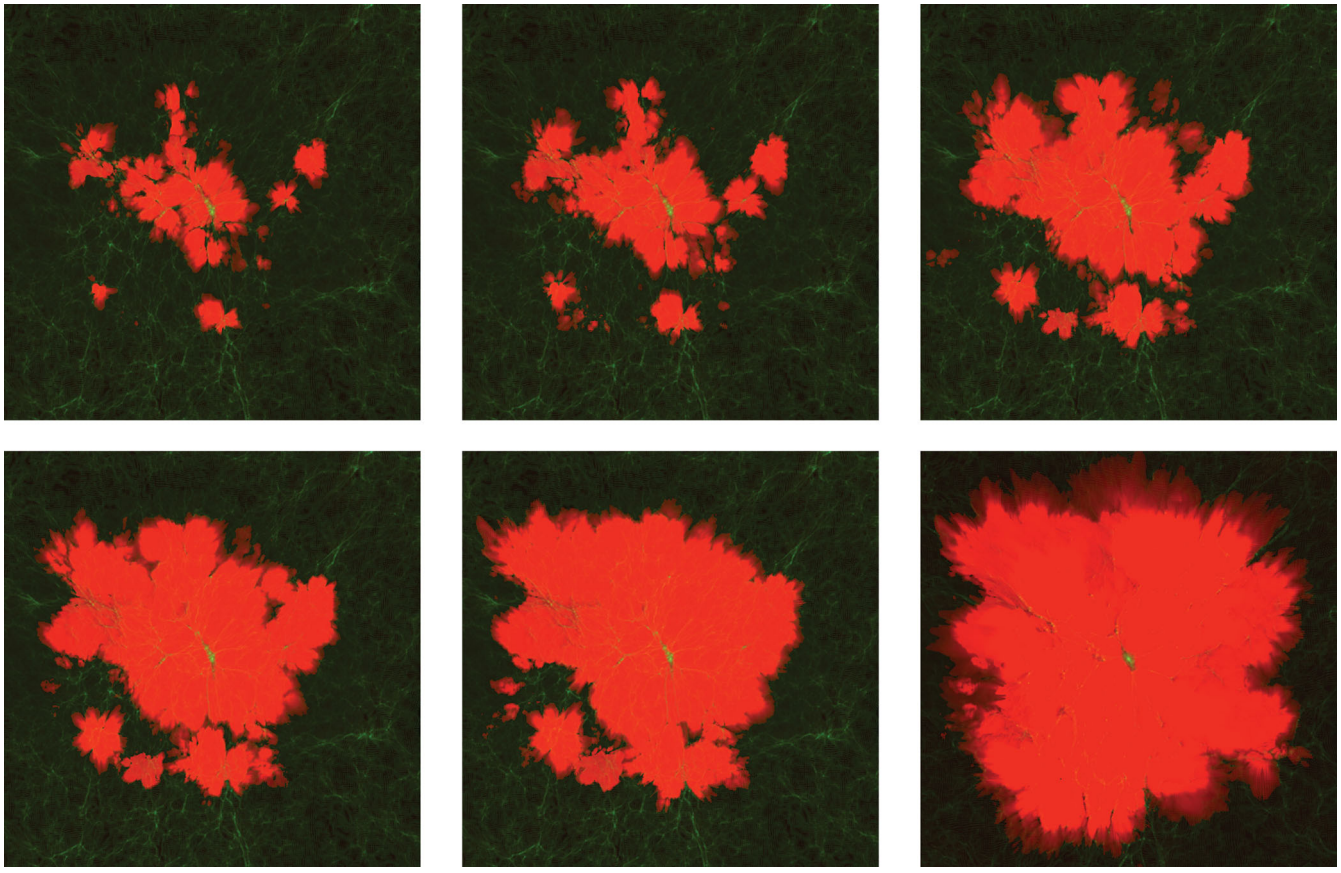

Figure 2. Snapshots of the ionization field for the six photoionization efficiencies tested in this study all taken at the same redshift ($z = 10.11$). Again, each panel represents a spatial slices (x–y projection), 460 h^{-1} kpc thick, of the ionized and neutral gas density from simulations of Model 1. Top left to top right: $f_\gamma = 150$, 250, 500 photons per baryon and bottom left to bottom right: $f_\gamma = 700$, 1000 and 5000 photons per baryon. The box in each panel has a comoving width of 6 h^{-1} Mpc.

of ionizing photons are injected into the IGM resulting in greater suppression in the higher escape fraction models than the lower escape fraction models. This amount of suppression taking place is most significant at $z < 16$. There are no active sources in any of the models below $z = 8$ except for one lone source forming at $z = 5$ in the photon-poor, M1_512_ph150, model.

Fig. 4 shows the cumulative total of GCs forming indicating a factor of ∼3 difference in total number from the lowest ($f_\gamma = 150$ photons per baryon) to the highest ($f_\gamma = 5000$ photons per baryon) ionization efficiency. For comparison, there are 102 MPGCs in the Milky Way based on a metal-poor metallicity cut-off ([Fe/H] < -1; Harris 1996).

Table 4 shows the total number of objects formed and suppressed over the entire simulation for different photoionization efficiencies. As expected, there is a drastic dependence of the suppression rate on the ionization efficiency. The number of objects which form between the photon-poor ($f_\gamma = 150$) and photon-rich ($f_\gamma = 5000$) environments in our models differ by a factor of 2.7.

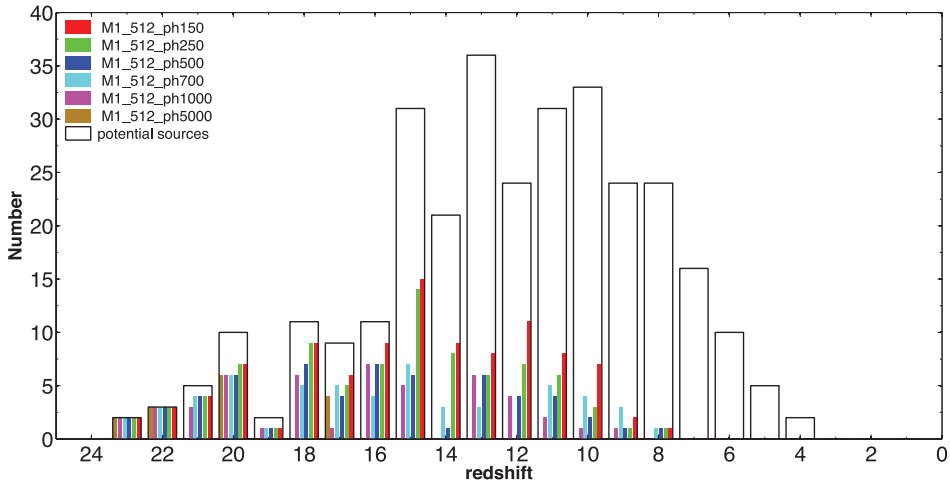

Figure 3. Formation histograms for each of the respective ionization efficiencies. The number of objects as a function of redshift are binned in whole integer redshifts for each snapshot of the simulation. For ever higher ionization efficiencies, more photons escape into the IGM, resulting in fewer objects forming at lower redshift (i.e. only those identified by the velocity–temperature criterion from Aquarius) due to an increased level of suppression. The clear histogram represents the formation of GCs without suppression included.

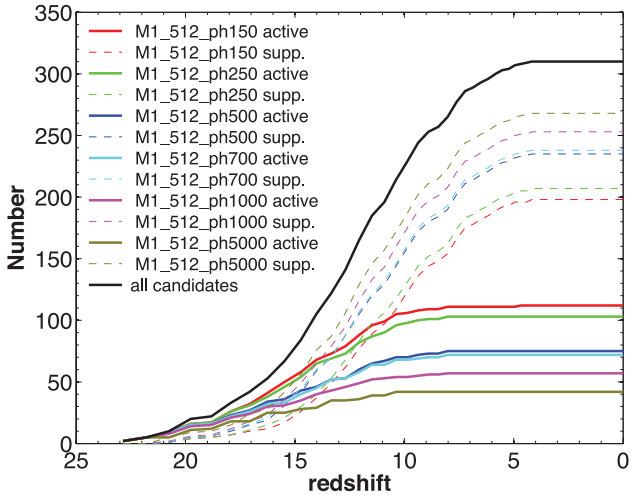

Figure 4. Cumulative formation history for each of the respective ionization efficiencies. The solid lines represent active sources and the dashed lines represent suppressed sources. The solid black line represents the formation of all potential cluster candidates identified within the Aq-A2 simulation.

Table 4. The number of active and suppressed sources of each of the various escape fractions and their corresponding suppression rates.

Model name	Number of Active GCs	Number of Suppressed GCs	Suppression Rate (fraction)
No suppression	310	0	0
M1_512_ph150	112	198	0.64
M1_512_ph250	103	207	0.67
M1_512_ph500	75	235	0.76
M1_512_ph700	72	238	0.77
M1_512_ph1000	57	253	0.82
M1_512_ph5000	42	268	0.86

4.1.3 Ages

As illustrated by the open bins in Fig. 3, the identification of GC candidates extends down to $z = 4$. Through the process of self-ionization, the potential number of GCs drastically decreases due to the ionization flux from the first group of active sources. This process pushes back the average age of each of the GC populations. The mean age (calculated assuming a flat cosmology) for Model 1 is shown in Table 5. Overall, a higher the ionization efficiency will lead to, on average, older GCs due to the wiping out of potential sources at low redshift. The youngest population on average is the population resulting from the M1_512_ph150 model, having an average age of 13.30 Gyr whilst the oldest population on average is the M1_512_ph150 model, having an average age of 13.42 Gyr. Whilst each of the model GC population's formation is extended in redshift space, the corresponding age range they occupy is quite narrow (mean = 13.39 Gyr, $\sigma = 0.04$ Gyr). The surviving GCs in all of the models have mean ages consistent with the Galactic MPGC ages determined from the Advanced Camera for Surveys carried out by Marín-Franch et al. (2009) (13.5 ± 1.5 Gyr) and other MPGC age studies ($z > 5$; Fan et al. 2006).

Table 5. Mean formation redshift and percentile ages for our MPGCs candidates in each model (assuming a flat cosmology).

Model name	$z_{\rm mean}$ formation	Percentile age (Gyr) 10 per cent	50 per cent	90 per cent
No suppression	12.25	12.82	13.20	13.36
M1_512_ph150	12.92	12.87	13.23	13.36
M1_512_ph250	13.31	12.92	13.25	13.38
M1_512_ph500	13.56	12.94	13.25	13.39
M1_512_ph700	13.75	13.01	13.25	13.39
M1_512_ph1000	13.92	13.01	13.27	13.39
M1_512_ph5000	14.05	13.01	13.27	13.39

4.1.4 Spatial distribution

Fig. 5 shows the $z = 0$ radial distributions of the GCs in our simulations in both raw number and as a fraction of the total number. These were obtained by following the most bound particle of each of the candidates once they had merged with the central halo through to the present day (see Section 3.2 for details). We find that there are few surviving candidates within 50 kpc of the host. Even for the

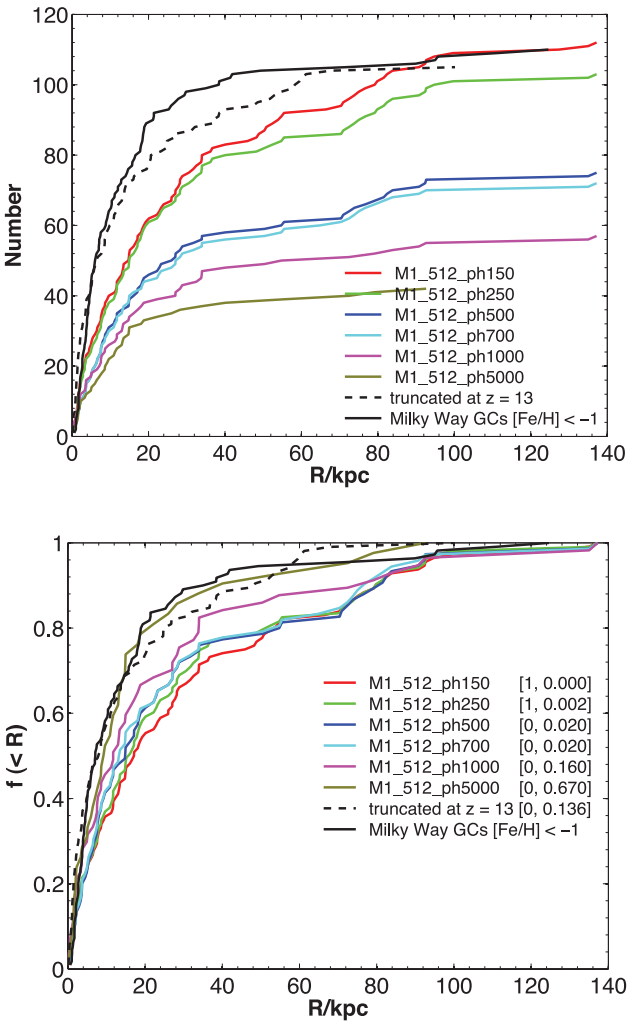

Figure 5. Radial distribution of candidate GCs in both raw number and normalized to the total number. The thick black line represents the Milky Way's MPGC distribution. In addition to the six ionization models, the black dashed line represents the truncation model (i.e. GCs in the sample have formed before $z = 13$ and have merged with the central halo by $z = 0$). The legend also shows the results from a two-sampled KS test carried out between the Milky Way metal-poor distribution and each of the respective models. Each number corresponds to $[H, p]$ where $H = 1$ if the test rejects the null hypothesis that they are drawn from the same distribution at the 1 per cent significance level and p is the asymptotic p-value.

most conservative reionization model (M1_512_ph150), there are ∼20 too few objects to reconcile the radial distribution of the AqA2 halo's MPGC distribution with that of the Milky Way.

Another significant feature is the difference in shape of the radial distributions of the inhomogeneous ionization models (i.e. models using C^2-RAY) and the truncation model (i.e. using $z_{\rm trunc}$). The truncation model's additional GC numbers in the central region originate from the inclusion of *all* potential sources before $z = 13$ which are unavailable to the models using C^2-RAY. As Fig. 3 illustrates, there are a number of potential sources between $z = 23$ and 13 which are otherwise suppressed in the inhomogeneous ionization models. These haloes, having been included in the candidate sample in the truncation model reveal themselves in the central regions of the spatial distribution at $z = 0$. This highlights the first, primary result of this work which is that by treating the ionization field in an inhomogeneous manner, it results in significantly different total numbers and $z = 0$ radial distributions of potential GCs when compared to a model adopting arbitrary truncation.

A Kolmogorov–Smirnov (KS) test carried out by comparing the six C^2-RAY distributions against the Milky Way MPGCs ([Fe/H] < -1) found that all models except the M1_512_ph150 and M1_512_ph250 models are inconsistent with the Milky Way MPGC distribution at the 1 per cent confidence level. It must be restated that none of the models are designed to replicate the distributions of the Milky Way and these results only show that these two of the six distributions (photon-rich models) are statistically consistent with the Milky Way's MPGC system.

The time-scale for dynamical friction (Chandrasekhar 1943) is inversely proportional to mass, so the GCs will be more affected by this process than the dark matter particles (which are of the order of 100 times less massive). For GCs of mass a few times $10^5 {\rm M}_\odot$ at radii of 10 kpc the dynamical friction time-scale is 10^{12} yr, so this is unlikely to affect our results.

4.1.5 Contribution to ionization of IGM

Fig. 6 shows the enclosed mass and volume ionized of each of the six models within a comoving box width (centred on the host galaxy) spanning 1–6 h^{-1} Mpc. Within the largest box size, the amount of volume and mass ionized is small compared to the amount of volume and mass ionized in a small box. This is because candidate formation density is largest in the central most dense region of the simulation. Since a large box width encloses significantly more baryons than a small box, the total volume and mass fraction ionized is lower. As the box width decreases, the amount of volume and mass ionized increases as expected. Similarly as the photoionization efficiency (f_γ) increases, the fraction of volume and mass of the respective enclosed volume also increases as expected. In the extremely photon-rich model (M1_512_ph5000), as much as 80 per cent of the entire simulated is ionized by $z = 10$.

In terms of volume, 60 and 98 per cent of the $2^3\ h^{-3}$ Mpc^3 volume centred on the AqA halo is fully ionized by $z = 10$ for the photon-poorest (M1_512_ph150) and photon-richest (M1_512_ph5000) models, respectively. In terms of the total mass ionized, 50 and 90 per cent of the total mass within the same volume was ionized by $z = 10$ for the photon-poor and photon-rich models, respectively (see Fig. 7). The subsequent decrease in the ionized mass fraction is due to the material recombining at low redshift.

The number of ionizing photons emitted by all active sources is plotted in Fig. 8. The most efficient of our models peaks at 10^{70} photons being produced over the course of the simulation. The active sources in our photon-poorest model produces approximately $10^{68.5}$ photons within the total $6^3\ h^{-3}$ Mpc^3 volume.

The primary result from this analysis is that if MPGCs did form via the mechanism tested, then at worst, MPGCs contributed a *non-trivial* fraction (≥40 per cent, Fig. 7) of the total ionization of the IGM within a distance of ∼1 h^{-1} Mpc of the Milky Way.

4.2 Model extension 1: dynamical disruption

We used the dynamical disruption model of Baumgardt & Makino (2003) to estimate the survival rates of MPGCs once they merge into the central host halo (as described in Section 3.2). Objects with dissolution times less than the look-back time to when they merged with the host are disrupted.

The sample includes all candidate clusters identified via the temperature–velocity dispersion threshold discussed in Section 2.2.

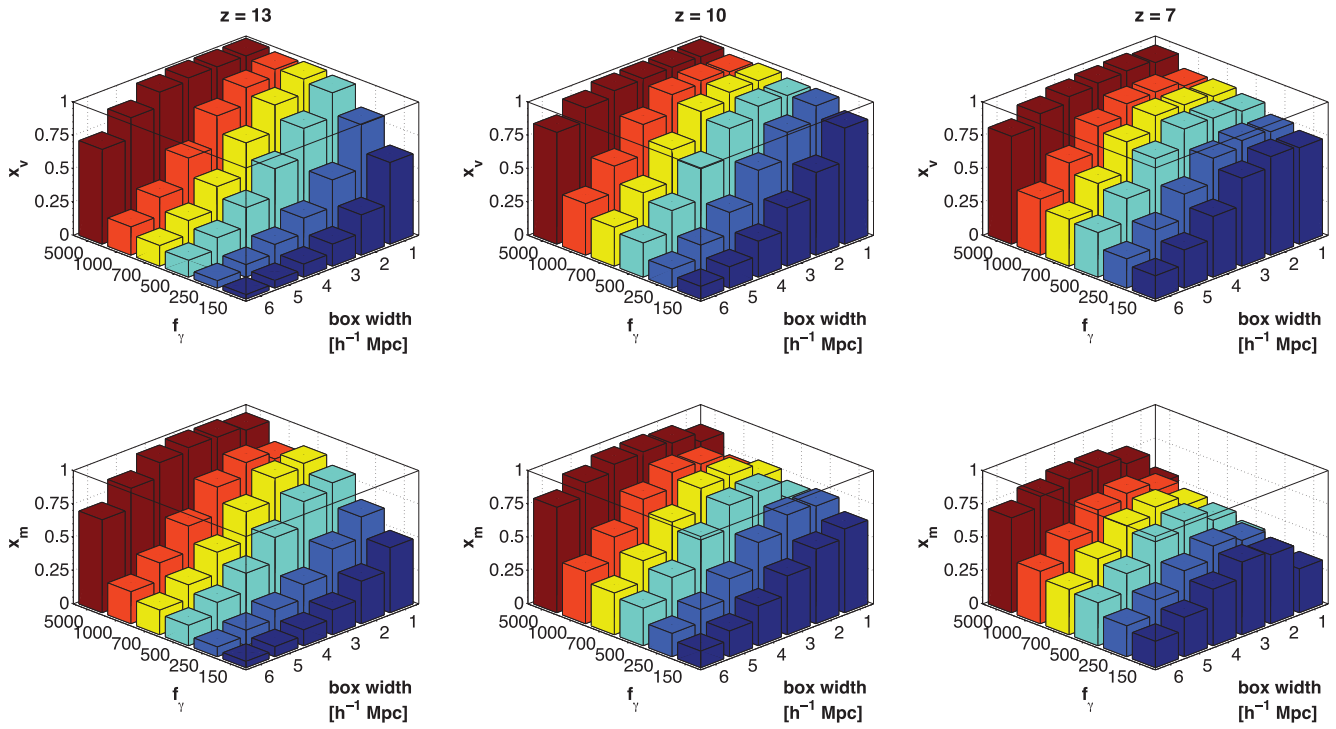

Figure 6. The fraction of the volume (x_v) and mass (x_m) ionized at three different redshifts ($z = 7$, 10 and 13) plotted simultaneously against the six different photoionization efficiencies (f_γ) and the width of the box surrounding the host halo in comoving coordinates. For each of the models, at a given redshift, a box was drawn around the central host galaxy (to within the nearest cell) and the volume and mass fraction ionized was calculated. Clearly, if MPGCs do form via the dark halo formation channel then their contributions to the ionization of their formation environments is substantial. Interestingly, at low box widths, the ionized mass fraction drops. This is because the number of baryons drastically increases towards the central regions and so the ionizing photons can not penetrate the inner regions of the halo. As discussed in Section 2.3.2, the source sample could be incomplete at distances greater than 2 h^{-1} Mpc from the host (i.e. box width >4 h^{-1} Mpc) due to the fact the high-resolution volume from which the candidates are identified is smaller than the total box volume of C^2-RAY (the density field is still accurately represented at all scales, however).

As shown in Fig. 9, just over half (60 per cent) of the clusters identified, whether they are suppressed or not, will undergo dynamical disruption. Further analysis of different King profiles indicated only a marginal (±6 per cent) swing in survival probability.

Fig. 10 presents a percentage break down of what happens to the sources that do not survive through to the present day. The only two ways of removing sources in this model is by dynamical disruption or suppression by ionization. With the exception of the photon-richest model ($f_\gamma = 5000$), approximately half of the candidate GCs in each model are lost due to dynamical disruption and just under half are lost due to suppression via photoionization. The reason the suppressed fraction does not increase more significantly as the ionization efficiency increases is because the sample only examines the subpopulation of clusters which are *destroyed* (i.e. all candidates of the initial population which were removed via suppression or disruption). For example, in the less efficient models, more clusters are going to be included in the sample because fewer clusters are suppressed at lower redshift. This also means however that a larger percentage of these clusters are susceptible to disruption.

The drastic decrease in the number of potential clusters (excluding the effect of suppression) has significant effects on the spatial distributions of the potential MPGC candidates. Fig. 11 plots the radial distribution of each of the models with and without dynamical disruption. Unlike the original model, none of the disruption models are statistically consistent Milky Way MPGCs at a 1 per cent significance level.

In order to gain a more complete understanding of the dynamical processes occurring within the host galaxy after a merger takes place, a full hydrodynamic, high-resolution simulation would be required in order to properly determine the survival rates of GCs. Other caveats of this work are described in Section 5.4. We present these broad brush dynamical destruction results to show, in concept, that large quantities of GCs will be destroyed once they merge with the central host galaxy and that their radial distributions are currently irreconcilable with the present-day metal-poor Galactic GC population.

4.3 Model extension 2: delayed GC formation

In this section, we examine our delayed model of GC formation (detailed in Section 3.1). The difference is that all suppressed candidates are still potential sources provided they (a) enter a neutral region of the IGM and (b) have *no* active ancestors. Utilizing the merger trees of the AqA2 halo enabled us to implement this model in a relatively straight forward manner.

Fig. 12 compares the formation history of the MPGC candidates in both the permanently suppressed and delayed formation models in relation to their present-day and formation galactocentric radii. At early times, the source positions between the two models are in exact agreement with one another (red stars within black circles) since the IGM has not begun to be significantly ionized. As the ionizing flux from those first objects increases over time, the number of suppressed candidates also increases, resulting in a number

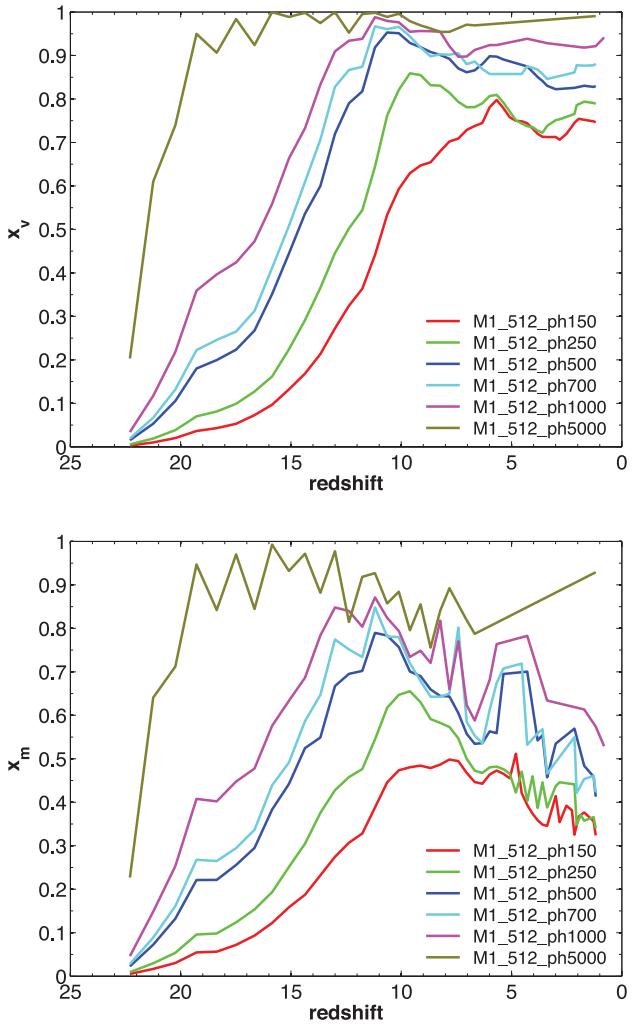

Figure 7. Redshift evolution of the volume (x_v) and mass (x_m) fraction ionized within a 2^3 h^{-3} Mpc^3 box centred on the host galaxy for each of the respective photoionization efficiencies. Whilst a significant quantity of the enclosed volume is ionized across each of the models, recombinations at low redshift decrease the mass fraction ionized since the number of active sources below $z < 10$ drastically reduces. In the late reionization era, overlap by neighbouring ionizing sources would ensure that the remaining neutral gas becomes ionized by $z = 0$ (see Iliev et al. 2011).

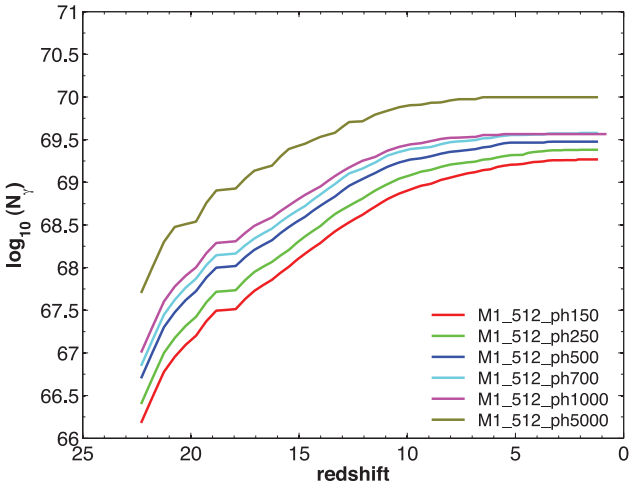

Figure 8. Cumulative number of ionizing photons emitted by MPGC candidates within Aquarius over the course of the simulation.

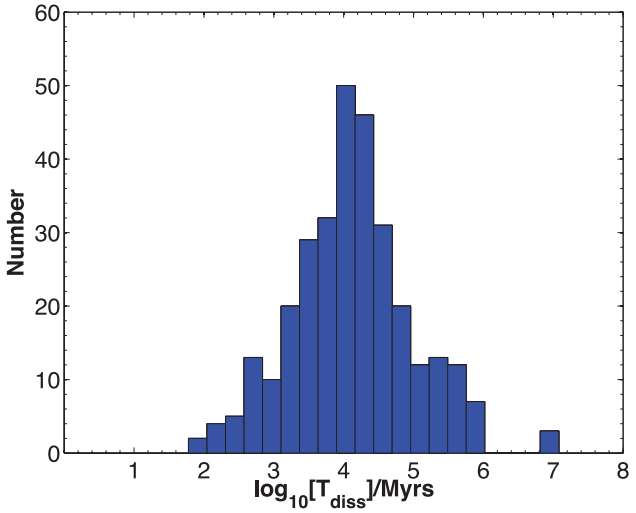

Figure 9. Dissolution time of candidate MPGCs which have merged with the central host by $z = 0$. An object with a dissolution time less than the look-back time it merged with the central host is disrupted.

of extra potential sources which could become active later if the environmental requirements are satisfied. The first of these sources becomes noticeable at $z \sim 19$ whereby a few previously suppressed haloes become active. Due to the non-linear nature of the ionizing field, these first additional sources then lead to more significant changes at later times. The majority of delayed candidates activate at $z < 8$ within a galactocentric distance of $R < 300$ h^{-1} kpc. This is a result of there being a large neutral region in the centre due to the recombination rate being larger than the ionization rate. This neutral region can also be reasonably seen upon a visual inspections of the central region in Fig. 2. It is clear that previously suppressed sources are merging into these regions and subsequently meeting the necessary environmental requirements to become active.

Fig. 13 compares the $z = 0$ radial distributions of all of the candidate MPGCs (cumulative and normalized) in both the permanently suppressed and delayed formation models. The immediate noticeable difference is the increase in the number of objects in the central region ($R < 40$ kpc) in the delayed model when compared to Model 1 of the same ionization efficiency. As indicated in Fig. 12, the majority of these new candidates are coming from suppressed sources becoming active in within 300 kpc of the host. These delayed haloes subsequently merge with the host galaxy and populate galactocentric distances between 0 and 100 kpc. Despite the extra GCs are small galactocentric radio, a KS test carried out on all six Model 2 distributions rejects the null hypothesis that they are drawn from the same distribution as the Milky Way MPGCs at the 1 per cent significance level.

Fig. 14 compares the $z = 0$ radial distributions of all of the candidate MPGCs in the delayed formation models (solid lines) and the same objects truncated at $z = 10$ (dashed lines). Whilst the delayed model candidates are far too extended in their entirety, when they are truncated their spatial distributions are more closely consistent with the MPGCs of the Milky Way (excluding the M1_512_ph5000). This suggests that if MPGCs did form via the dark halo formation channel, then either external ionization (i.e. ionization from the

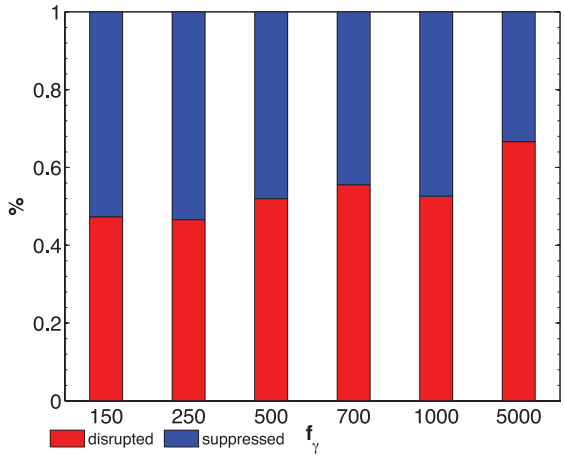

Figure 10. Accounting for the empty or disrupted haloes. Each stacked bar represents the percentage fraction lost due to suppression and dynamical disruption. With the exception of the photon-richest model ($f_\gamma = 5000$), approximately half are consistently lost due to disruption and just under half are lost due to suppression in each of the respective models.

Local Group) or ionization from other unaccounted for sources (e.g. Population II stars) must dominate the local environment from $z = 10$ onwards in order for their radial distributions to be consistent with that of the Milky Way.

5 DISCUSSION

Here, we discuss the more general achievements and limitations of our models with a particular emphasis on areas of improvement.

5.1 Overview

In our previous relatively simple GC formation model (G10), we found that if GCs could have formed (in part) at the centre of dark halo potentials, then the contributions of MPGCs stemming from these dark haloes to the reionization of the IGM was significant. Using the cumulative mass of these primordial GCs, we estimated their ionizing flux and came to the conclusion that it would have been possible for GCs to have ionized the entire Milky Way by $z = 13$ (for $f_\gamma = 210$). Despite the success of this model, it had several limitations. For example, (a) 100 per cent of the ionizing flux coming from each GC was assumed to have gone into ionizing the Milky Way, (b) only one value for the emissivity of the GCs was examined, (c) the state of the IGM was entirely unknown at high redshifts and (d) an arbitrary truncation redshift based on relatively naive assumptions about the nature of the IGM.

Our current model improves on all of these areas. The first immediate difference is that the ionization field emanating from the sources is inhomogeneous. This reveals itself in both the visuals of Fig. 1 and the extended formation histograms in Fig. 3. Another key feature of Fig. 3 is that unlike the formation history in G10 and Bekki et al. (2008), MPGC formation is extended in time rather than abruptly ending at one specific redshift. This extended formation can only come about due to the inhomogeneous way in which the ionization field propagates through the bulk IGM. Our models are consistent with the overall picture of extended reionization. For the photon-poorest model (M1_512_ph150), the last source is activated as late as $z = 4$ whereas in the most photon-rich model (M1_512_ph5000), MPGCs cease forming by $z = 7$ (see Table 5).

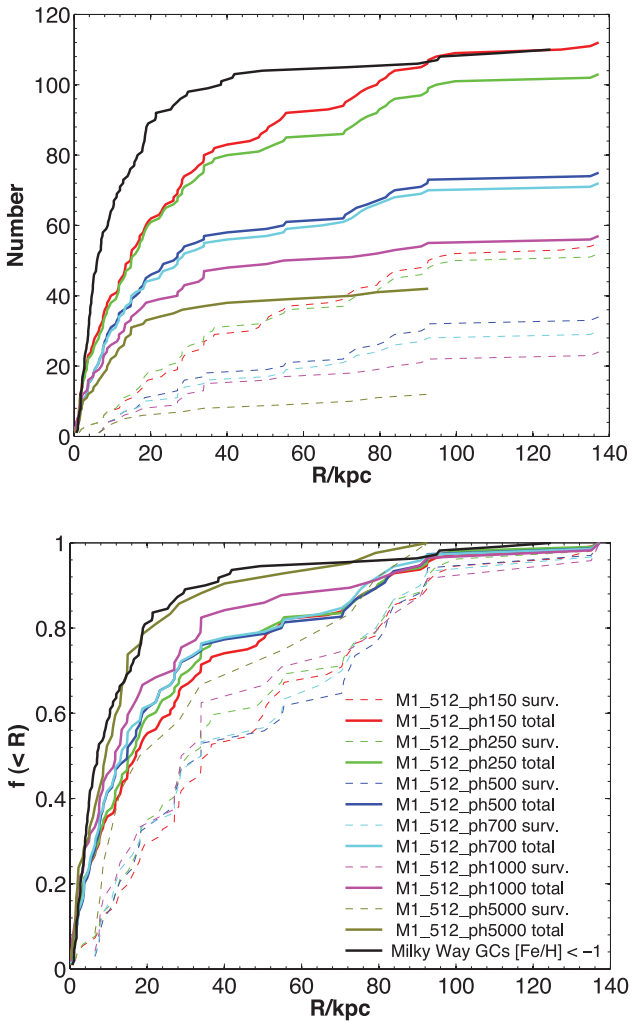

Figure 11. Model 1 (permanent suppression) radial distributions of candidate MPGCs in both raw number (top panel) and normalized number (bottom panel) for models with (dashed lines) and without (solid lines) dynamical disruption. The effect of the dynamical model is stark. Candidate GC populations in the central regions are drastically reduced resulting in far more extended radial distributions. For reference, the upper panel has the same legend as the lower panel but we exclude it for clarity.

5.2 GC dark halo formation hypothesis

Whether or not MPGCs originally formed within dark matter haloes is still an open question. In this work, we do not necessitate that they do but rather ask what sort of estimations can one derive if the dark matter halo formation channel produces distributions similar to observations. It must be reiterated that our conclusions are based on the assumption that the dark halo formation hypothesis is an accurate model of how MPGCs formed.

We conclude that although some GCs may have formed in dark matter haloes and were subsequently stripped upon merging with the central host galaxy, a portion of the Galactic GC population we observe today may have come about by other means (e.g. mergers, giant molecular clouds, tidal tails). If MPGCs did form via one or more of other mechanisms, a quantitative

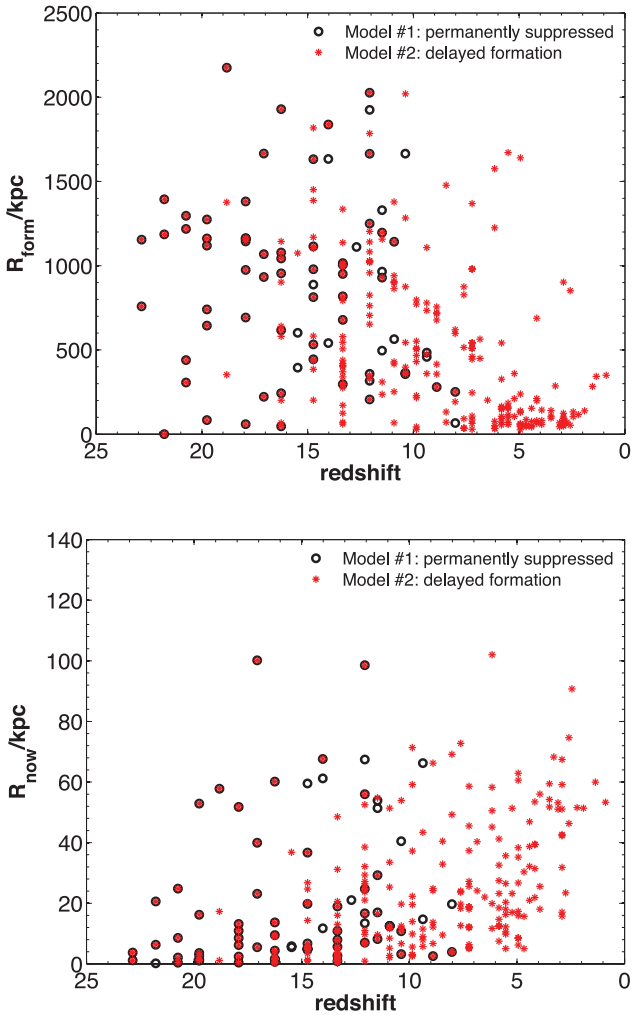

Figure 12. Top panel: comparison between Model 1 (permanently suppressed, solid black circles) and Model 2 (delayed formation, red stars) using their respective comoving galactocentric distance at formation and their redshift of formation. Bottom panel: similar to the top panel but this time shows the galactocentric distance at $z = 0$ and redshift of formation of each of the candidates. There are extra sources forming at $z < 8$ in Model 2 due to previously suppressed sources becoming active after meeting the necessary environmental conditions within $R < 300\ h^{-1}$ kpc of the host galaxy.

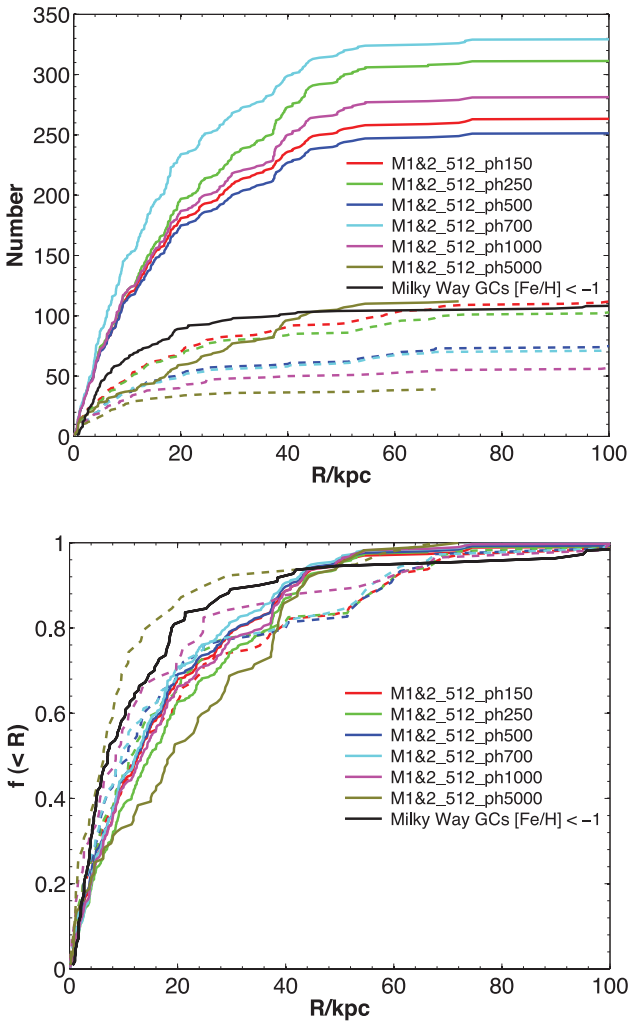

Figure 13. Cumulative (top panel) and normalized (bottom panel) radial distributions of all photoionization efficiencies in both Model 1 (permanently suppressed, dashed) and Model 2 (delayed formation, solid). The delayed model adds as much as three times more potential GC candidates than the equivalent f_γ permanently suppressed model (Model 1).

analysis of their contributions to the reionization of the IGM is still required.

In Model 1, even before including effects like dynamical disruption, the radial distributions are either too shallow or do not contain enough GCs to reproduce the Milky Way distribution (even if one assumes several GCs formed per dark matter halo). Though the delayed model (Model 2) does increase the number of potential sources, a great majority of them do not populate the required locations in order to reconcile the simulated distribution with the Milky Way MPGC distribution. This however ignores the contribution from external sources inundating the IGM with ionizing photons which would suppress low-redshift GCs. If we adopt Model 2 *and* truncate sources at $z = 10$, the spatial distributions are consistent with that of the Milky Way MPGCs.

5.3 Convergence

An important concern for the models is that the results are not dependent on the resolution of the particular simulation used. G10 has already shown that the identification of sources is not resolution limited by comparing the formation history of objects found within the higher resolution AqA2 halo to the lower resolution AqA3 halo. Here, we are interested in the dependence of the results on the resolution used by C^2-RAY. In conjunction with each of the 512^3 suite of models, a lower resolution 256^3 simulation was carried out on our fiducial model (M1_512_ph500) to test for convergence. In Fig. 15, we present the formation history of MPGCs in our fiducial model at both resolutions, 256^3 and 512^3. Both models are in excellent agreement with one another varying only by few per cent in number. A KS test also verifies that they are consistent with having been drawn from the same distribution at the 5 per cent significance level. This agreement shows that the results are not significantly biased by the resolution of the simulations used.

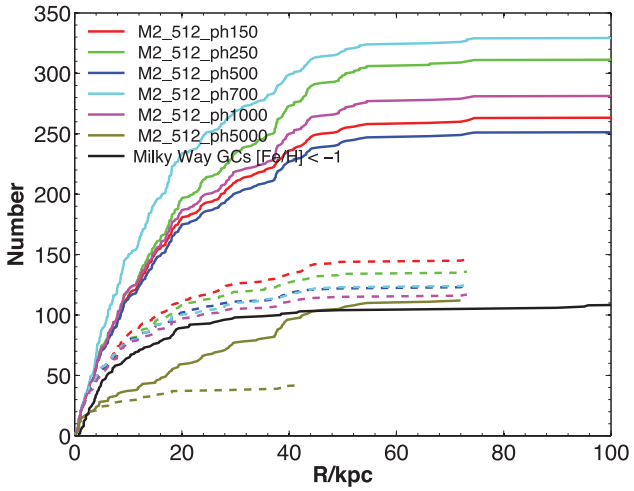

Figure 14. Radial distributions of all photoionization efficiencies in Model 2 (solid) and the same objects truncated at $z = 10$ (dashed). This shows that a better match to the Milky Way can be obtained if further sources of ionization are added at late redshifts.

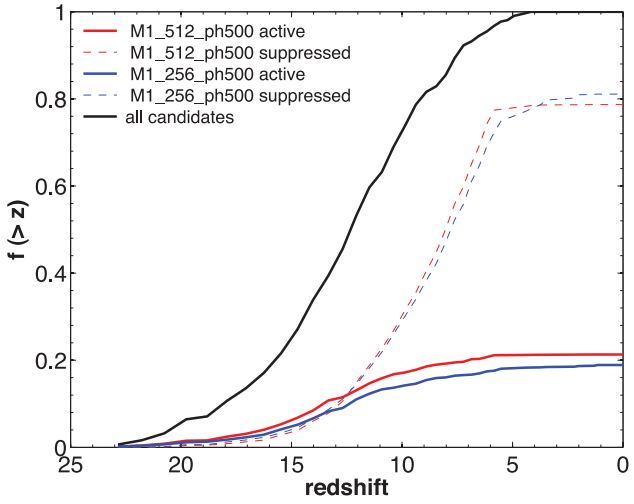

Figure 15. Convergence test for our fiducial model, M1_512_ph500. In terms of the cumulative formation number, the lower resolution, 256^3, mesh shows a near-complete agreement with the higher resolution 512^3 mesh. A KS test reveals that the hypothesis that they are drawn from the same distribution cannot be rejected at the 5 per cent significance level.

5.4 Caveats of this work

Although we have tried to eliminate as many known weaknesses of the models used in this study, there are still a number of remaining caveats which need to be addressed in future studies to improve upon this work.

(i) *Accountability of the ionization sources:* whilst the majority of the local ionizing flux will come from low-mass dark matter haloes in the early Universe as time evolves, each of our models diverges from an accurate account of the *true* ionizing sources. This is because field stars, non-dark-matter-dominated giant molecular clouds and other such objects will begin to play a dominating role at lower redshifts which are not yet modelled in the current work. Indeed, recent work by Iliev et al. (2011) and Alvarez et al. (2009) suggests a reionization overlap scenario for the local Milky Way volume whereby reionization was kick-started by low-mass sources locally, but their effective flux is superseded by the ionizing flux of the Local Group. Nearby proto-clusters (e.g. Virgo and Fornax) clusters would also have had an appreciable effect at later times.

(ii) *Unmerged GCs*: throughout this work, we have limited our sample to include only those which have merged with the central halo by $z = 0$. This was done to not only ensure an accurate sample but for simplicity. Candidates which do not merge with the central halo by $z = 0$ could be Galactic dwarf galaxies as they will have retained their dark matter haloes, though this is highly speculative. Fig. 10 of G10 shows that the spatial distribution of these non-merged objects is consistent with those GCs found surrounding neighbouring dwarf galaxies (see Mateo 1998). Overall there are 47 distinct haloes containing 68 GCs at $z = 0$, indicating that there has been not only major merging with the central host, but also minor merging of GCs with proto-dwarf galaxies. Whilst there is sufficient research to suggest that GCs could have formed in dark matter haloes and were subsequently stripped of their outer envelope, it remains unclear where the degeneracy breaks between GC and dwarf galaxy formation processes. An examination of these non-merged objects needs to be carried out in a more detailed manner to determine their connection (if any) to the known dark matter-dominated satellites of Milky Way.

(iii) *GC formation efficiency*: all of the work presented here assumes that for every dark matter halo, exactly one GC will form in the centre of its potential well. Given that fragmentation of large gas clouds can lead to multiple stellar populations within a single dark matter halo, it still remains unclear as to exactly how many GCs will form in a given dark halo. In any case, it would only shift the halo-centric radii plots upwards and not really have any impact on the structural properties of the distributions. Understanding GC formation efficiencies better will lead to better estimates of their overall numbers if they do form via the dark halo formation channel.

(iv) *Statistical limitation using one Aquarius halo*: perhaps one of the biggest drawbacks of this work is that it only examines one Milky Way-type galaxy. In order to get a better understanding of the underlying physics involved, a larger sample of Milky Way-type galaxies would be required. The statistical variation in the number of satellites in the Aquarius simulation has also been shown to vary by a factor of 2 or more (Lunnan et al. 2012). The overall conclusion that GCs contributed a non-trivial amount to the reionization of the local IGM would be unlikely to change given that the most conservative of our models reionizes more than 50 per cent both by mass and volume of the local IGM by $z = 10$ (see Fig. 7). Although the Aquarius suite consists of six such simulations, the logistics behind analysing the remaining five haloes is not feasible at this time.

(v) *Treatment of dynamical disruption*: the exact nature of the dynamical processes inside the central host halo after a halo merges is inherently difficult to treat properly. In our model, we trace the single most bound particle of the in-falling MPGCs. These trace particles could be susceptible to violent dynamical changes within the halo resulting in spatial distributions that might not necessarily reflect where the true $z = 0$ position of the baryonic content ended up. In an improvement to this, one could trace the 10 per cent most bound particles to get a better hold on the $z = 0$ position of the clusters under study. A better understanding of the disruption processes is a critical component of linking high-z formation processes to $z = 0$ properties (e.g. at least half of the original GC population to have formed at high redshift is destroyed by tidal disruption alone).

(vi) *Dependence on ionization cell-fraction threshold*: since our simulations do not (yet) have gas and do not calculate the

temperature, we use the local ionized fraction as a proxy for the temperature (which has a few uncertainties). At very high redshifts, things are reasonably simple since it is typically a simple transition from largely neutral to almost completely ionized as the ionization front overruns the cell in question. A noted problem is what to do after this point. Since the ionization suppresses the low-mass sources, some regions start to recombine (and cool), which eventually should allow the formation of low-mass sources again, but the question is when does this occur? This is a source of uncertainty and so a number of cell-fraction thresholds need to be tested in future work. At the moment, the cell fraction ($x_{\rm thresh}$) was set to 0.1 for this work but arguments can be made to raise this threshold to higher values of $x_{\rm thresh} = 0.5$ or even 0.9 (see Appendix B of Iliev et al. 2011). Model 1 should be retested using these thresholds to determine how much stochasticity one would expect from varying this threshold.

(vii) *Clumping*: volume-averaged recombination rates in an inhomogeneous IGM scale with the clumping factor $C = \langle\rho^2\rangle/\langle\rho\rangle^2$, where the ρ denotes volume-averaged densities. In our work, we set $C = 1$ (no clumping). The dependence of halo suppression for varying degrees of clumping is as yet unknown but will be implemented in subsequent work. We also do not advect the gas between cells in the IGM which needs to be carried out if this work is to improve.

Recently, Spitler et al. (2012) combined observations with novel modelling to detect evidence of inhomogeneous reionization by MPGCs on cluster scales. They exploited a fundamental characteristic of galaxy assembly (i.e. spatial biasing and kinematics of MPGCs) to constraint the local reionization epoch around individual galaxies. They found a joint constraint from three galaxies of $z_{\rm reion} = 10.5^{+1.0}_{-0.9}$ which agrees well with the latest *Wilkinson Microwave Anisotropy Probe* constraint on $z_{\rm reion}$. Interestingly, they also found a 1.7σ indication that low-density environments were reionized before medium- and high-density environments. These results are consistent with the theory that reionization was prolonged in duration with neutral-gas surviving in high-density environments for extended periods. The redshift range of reionization of the local IGM in this work is consistent with their results to within 1σ.

Only recently, have computational developments made possible the ability to simulate vast cosmological volumes with exquisite resolution. Future studies such as the work in this paper could be applied to high-resolution cluster environments to verify the claims made by Spitler et al. (2012). Preliminary work will be carried out on the Millennium II simulation but more tailored simulations for this type of study would be desirable.

6 CONCLUSIONS

We draw the following important conclusions regarding the reionization of the IGM by metal-poor GCs from this work.

(i) Treating the ionization field in an inhomogeneous manner results in substantially different numbers and spatial distributions. Our basic model adopting this type of treatment produces comparable numbers of GC candidates to that of the Milky Way but results in radial distributions which are too shallow. Whilst this model does not rule out possibility of GCs forming inside dark matter haloes at high redshift, it does indicate that GCs must have formed via other mechanisms to account for the lack of numbers at low radii in our model.

In our so-called delayed model where GCs are able to become active after having been previously suppressed, the number of candidate GCs drastically increases. These additional candidates however do not end up residing within the inner $R < 60$ kpc of the host halo at $z = 0$ and so the resulting radial distributions are still not comparable to that of the Milky Way.

In the arbitrary truncation model, the radial profiles and numbers are comparable to the Milky Way MPGCs. This is because in the truncation model (a) there are extra sources available at high redshift which boosts the number of sources at small radii and (b) it, by definition, totally removes the sources below $z_{\rm trunc}$ which reduces the number of sources at large radii. This ultimately shows that realistic populations can be produced if external sources dominate the photon budget at later times.

Overall, the more sophisticated work in this paper clearly shows that treating the ionization of the local IGM in a spatially inhomogeneous manner leads to the IGM being reionized at different places at different times which greatly impacts the radial distributions of MPGCs.

(ii) GCs injected high numbers of ionizing photons into the IGM at high redshift. Conservative efficiency estimates of $f_\gamma = 150$ photons per baryon would have resulted in MPGCs ionizing more than 50 per cent of the local IGM mass and 60 per cent of the local IGM volume by $z = 10$ (within an enclosed volume of $2^3\ h^{-3}$ Mpc^3 centred on the host) and upwards of 98 per cent of the volume and 90 per cent of the mass for the photon-richest model ($f_\gamma = 5000$ photons per baryon). We also estimate that as many as 10^{70} photons (minimum: $10^{68.5}$ photons) were injected in the IGM from MPGCs alone during the early build-up of the Milky Way. Such a quantity of photons would surely impact the formation of structures around not only the Milky Way, but other GC-rich environments as well.

(iii) The suppression rate of MPGCs in our simplest reionization model (M1_512_ph150) was 36 per cent of a total 310 possible MPGC sources. The number of objects which form between the photon-poor ($f_\gamma = 150$) and photon-rich ($f_\gamma = 5000$) environments differs by a factor of 2.7.

(iv) The unsuppressed MPGCs in all models have a narrow age range (mean = 13.34 Gyr, $\sigma = 0.04$ Gyr) consistent with current ages estimates of the Milky Way MPGCs.

(v) The radial distributions for the M1_512_ph150 and M1_512_ph250 models were the only distributions to be statistically consistent with the distribution of the Milky Way MPGCs at the 1 per cent significance level.

(vi) In an extension to Model 1, we found that dynamical destruction destroys nearly half (52 per cent) of the total GCs available resulting in a sample of GC candidates which is much smaller in number when compared to the Milky Way MPGCs. A KS test carried out on all six Model 2 distributions rejected the null hypothesis that they are drawn from the same distribution as the Milky Way MPGCs at the 1 per cent significance level.

(vii) Allowing suppressed haloes to turn on once they satisfy the required environmental conditions results in double and some times triple the number of potential GCs having formed. These 'delayed GCs' begin forming at $z \sim 19$ and continue to form up until the present day. The majority of these objects however form within neutral-gas regions of the simulation volume at $z < 8$ and at $R < 300\,h^{-1}$ kpc from the host. Due to their late formation times, these objects are most likely self-enriched and are therefore not suitable for comparison to the Milky Way MPGCs. If we impose truncation at $z = 10$, the photon-rich radial distributions ($f_\gamma = 1000$–5000 photons per baryon) are consistent with that of the Milky Way.

In summary, a number of avenues could be explored in future work. Measurements of the variation in our results across a wide variety of Milky Way-type haloes and a number of other sources of

reionization should be studied. Furthermore, testing a range of formation efficiencies, cell-fraction thresholds ($x_{\rm thresh}$) and an improved treatment of the dynamical disruption will help comprehend the ultimate origin of GCs and the role they played during the epoch of reionization.

ACKNOWLEDGEMENTS

We wish to thank Holger Baumgardt for many useful discussions relating to the dynamical models used in this work.

The simulations for the Aquarius Project were carried out at the Leibniz Computing Center, Garching, Germany, at the Computing Centre of the Max-Planck-Society in Garching, at the Institute for Computational Cosmology in Durham and on the 'STELLA' supercomputer of the LOFAR experiment at the University of Groningen.

This work was supported by funding from the Australian Research Council (grant number DP110102608) and the Science and Technology Facilities Council (grant number ST/F002858/1). ITL and PAT were partially supported by the Science & Technology Facilities Council (grant number ST/I000976/1). We also thank the Southeast Physics Network (SEPNet) for support. BG would like to acknowledge the support provided by the University of Queensland via a University of Queensland Postgraduate Scholarship.

REFERENCES

Alvarez M. A., Shapiro P. R., Ahn K., Iliev I. T., 2006, ApJ, 644, L101
Alvarez M. A., Busha M., Abel T., Wechsler R. H., 2009, ApJ, 703, L167
Barkana R., 2004, MNRAS, 347, 59
Baumgardt H., Kroupa P., 2007, MNRAS, 380, 1589
Baumgardt H., Makino J., 2003, MNRAS, 340, 227
Bekki K., 2005, ApJ, 626, 93
Bekki K., Yahagi H., 2006, MNRAS, 372
Bekki K., Yahagi H., Nagashima M., Forbes D. A., 2007, MNRAS, 382, L87
Bekki K., Yahagi H., Nagashima M., Forbes D. A., 2008, MNRAS, 387, 1131
Boley A. C., Lake G., Read J., Teyssier R., 2009, ApJ, 706, L192
Boylan-Kolchin M., Bullock J. S., Kaplinghat M., 2011, MNRAS, 415, L40
Bromm V., Clarke C. J., 2002, ApJ, 566, L1
Bromm V., Larson R. B., 2004, ARA&A, 42, 79
Busha M. T., Alvarez M. A., Wechsler R. H., Abel T., Strigari L. E., 2010, ApJ, 710, 408
Carretta E., Bragaglia A., Gratton R. G., Recio-Blanco A., Lucatello S., D'Orazi V., Cassisi S., 2010, A&AS, 516, A55
Chandrasekhar S., 1943, ApJ, 97, 255
Ciardi B., Stoehr F., White S. D. M., 2003, MNRAS, 343, 1101
Cole S., Helly J., Frenk C. S., Parkinson H., 2008, MNRAS, 383, 546
Conroy C., Loeb A., Spergel D. N., 2011, ApJ, 741, 72
Davidsen A. F., Kriss G. A., Zheng W., 1996, Nat., 380, 47
De Angeli F., Piotto G., Cassisi S., Busso G., Recio-Blanco A., Salaris M., Aparicio A., Rosenberg A., 2005, AJ, 130, 116
Fan X. et al., 2001, AJ, 122, 2833
Fan X. et al., 2006, ApJ, 132, 117
Ferrara A., Loeb A., 2012, preprint (arXiv:1209.2123)
Furlanetto S. R., Zaldarriaga M., Hernquist L., 2004, ApJ, 613, 1
Griffen B. F., Drinkwater M. J., Thomas P. A., Helly J. C., Pimbblet K. A., 2010, MNRAS, 405, 375 (G10)
Grillmair C. J., Freeman K. C., Irwin M., Quinn P. J., 1995, AJ, 109, 2553
Harris W. E., 1996, VizieR Online Data Catalog, 7195, 0
Iliev I. T. et al., 2006, MNRAS, 371, 1057
Iliev I. T., Pen U.-L., Bond J. R., Mellema G., Shapiro P. R., 2007, ApJ, 660, 933
Iliev I. T. et al., 2009, MNRAS, 400, 1283
Iliev I. T., Moore B., Gottlöber S., Yepes G., Hoffman Y., Mellema G., 2011, MNRAS, 413, 2093
Iliev I. T., Mellema G., Shapiro P. R., Pen U.-L., Mao Y., Koda J., Ahn K., 2012, MNRAS, 423, 2222
King I. R., 1966, AJ, 71, 64
Leitherer C. et al., 1999, ApJ, 123, 3
Loeb A., Barkana R., 2001, ARA&A, 39, 19
Lunnan R., Vogelsberger M., Frebel A., Hernquist L., Lidz A., Boylan-Kolchin M., 2012, ApJ, 746, 109
Madau P., Haardt F., Rees M. J., 1999, ApJ, 514, 648
Mapelli M., Ferrara A., Pierpaoli E., 2006, MNRAS, 369, 1719
Marín-Franch A. et al., 2009, ApJ, 694, 1498
Mashchenko S., Sills A., 2005, ApJ, 619, 243
Mateo M. L., 1998, ARA&A, 36, 435
Mellema G., Iliev I. T., Alvarez M. A., Shapiro P. R., 2006, New Astron., 11, 374
Moore B., 1996, ApJ, 461, L13
Moore B., Diemand J., Madau Pieroand Zemp M., Stadel J., 2006, MNRAS, 368, 563
Nishi R., 2002, Prog. Theor. Phys. Suppl., 147, 1
Ocvirk P., Aubert D., 2011, MNRAS, 417, L93
Odenkirchen M. et al., 2003, AJ, 126, 2385
Peebles P. J. E., 1984, Sci, 224, 1385
Power C., Wynn G. A., Combet C., Wilkinson M. I., 2009, MNRAS, 395, 1146
Rees M. J., 1997, in Tanvir N. R., Aragon-Salamanca A., Wall J. V., eds, The Universe at $z > 5$: When and How Did the 'Dark Age' End? p. 115
Ricotti M., 2002, MNRAS, 336, L33
Ricotti M., Ostriker J. P., 2004, MNRAS, 350, 539
Ricotti M., Shull J. M., 2000, ApJ, 542, 548
Schaerer D., Charbonnel C., 2011, MNRAS, 413, 2297
Sokasian A., Abel T., Hernquist L., Springel V., 2003, MNRAS, 344, 607
Spitler L. R., Romanowsky A. J., Diemand J., Strader J., Forbes D. A., Moore B., Brodie J. P., 2012, MNRAS, 2978
Springel V., White S. D. M., Tormen G., Kauffmann G., 2001, MNRAS, 328, 726
Springel V. et al., 2005, Nat, 435, 629
Springel V. et al., 2008, MNRAS, 391, 1685
Tumlinson J., Venkatesan A., Shull J. M., 2004, ApJ, 612, 602
Wise J. H., 2012, preprint (arXiv:1201.4820)
Wise J. H., Cen R., 2009, ApJ, 693, 984
Yajima H., Choi J.-H., Nagamine K., 2011, MNRAS, 412, 411

This paper has been typeset from a TEX/LATEX file prepared by the author.